Nanoscale

ROYAL SOCIETY OF CHEMISTRY

PAPER

View Article Online
View Journal | View Issue

Check for updates

Cite this: *Nanoscale*, 2025, **17**, 15301

How many electrons to stabilize the icosahedral Cu_{55} core in ligated nanoclusters? The example of $[Cu_{55}(NHC)_6]$†

Mohamed Amine Zerizer,[a,b] Christian Kleeberg,[c] Bachir Zouchoune *[a,b] and Jean-Yves Saillard *[d]

Received 7th April 2025,
Accepted 19th May 2025

DOI: 10.1039/d5nr01400j

rsc.li/nanoscale

While ligand-protected clusters with M_{55} icosahedral cores are rarely encountered so far, DFT calculations have been performed on a series of bare and ligated Cu_{55} clusters, including the structurally characterized $[Cu_{55}(IDipp)_6]$. Calculations indicate that the best closed-shell superatomic electron counts for such species are 48, 50, 52 and 56. None of them is a superatom "magic" number. The closest "magic" number, namely 58, which would correspond to full occupation of the 1G level, is highly disfavored. The 48, 50, 52 and 56 counts correspond to 1G partial occupations and can be rationalized from Jahn–Teller distortions away from R^3 or I_h symmetry. Similar calculations on related Au_{55} clusters provided comparable results, with the exception of the 52-electron count, which is not favored as a closed-shell with gold. Neutral ligands such as NHCs, are expected to stabilize efficiently the closed-shell 56-electron count, providing they are able to sterically screen all the "exposed" metal atoms.

1. Introduction

Atomically precise noble metal nanoclusters stabilized by ligands of various nature are arousing important scientific interest due to their various properties and unique structural chemistry. Their size, intermediate between that of simple molecules and nanoparticles, makes them chemically well-defined models for understanding at the atomic scale the structure and properties of metal nanoparticles which have ranges of size and shape distribution.[1–3] The stability of such nanoclusters can generally be rationalized within the superatom model,[4–6] which draws relationships between structure and number of metal "free" electrons.

A ligated nanocluster can be structurally divided into two parts, namely the metal core inside and its protecting outer shell at the periphery. The outer shell is composed of the ligands and possibly additional metal atoms which connect the ligands between them and, contrarily to the ligands, are loosely interacting with the core. In fact, strictly speaking the superatom model applies to the metallic core itself, providing that the latter is both sufficiently compact and spheroidal. This double condition is particularly well satisfied by the 13-atom centered icosahedron, whose compacity approaches that of the *fcc* or *hc* close-packing.[7] Such an $M@M_{12}$ spheroidal motif is predicted by the superatom model to be particularly stable when bearing 8 "free" electrons.[4–6] An emblematic example is $[Au_{13}(PMe_2Ph)_{10}Cl_2]^{3+}$, which was synthesized and structurally characterized in 1981 by Mingos, Welch and co-workers[8] and whose $[Au_{13}]^{5+}$ core contains 8 6s(Au) electrons, a "magic" closed-shell superatomic number.

Mackay has shown that a fairly compact packing can be preserved if one adds successive concentric shells of $(10i^2 + 2)$ atoms around the central $M@M_{12}$ icosahedron.[7] Such concentric shell arrangements follow what is called a geometrical shell-closure. Adding only one additional shell ($i = 2$) results in an $M@M_{12}@M_{42}$ assembly of 55 atoms (Fig. 1). As far as we know, there are only a few ligated M_n ($n > 55$) clusters containing this 55-atom motif embedded in a larger multi-shell assembly,[9–12] and there are only four structurally characterized ligated M_{55} species, plus one related hybrid $M_{54}Cl$ species. In this latter case, namely $[\{Ag@Ag_{12}@(Ag_{29}Cu_{12}Cl)\}(CCR)_{36}]^{3-}$, the second icosahedral shell surprisingly contains one chlorine atom in the place of a metal atom.[13] Considering it as an outer chloride ligand, one ends up with a count of 20 electrons, another "magic" closed-shell superatomic number.[13] One of the four true M_{55} species is Dahl's $[Pd_{55}(P^iPr_3)_{12}(\mu_3\text{-}CO)_{20}]$ cluster[14] which has been shown to be also a 20-electron

[a]*Unité de Recherche de Chimie de l'Environnement et Moléculaire Structurale, Université Constantine (Mentouri), 25000 Constantine, Algeria. E-mail: bzouchoune@gmail.com*
[b]*Laboratoire de Chimie appliquée et Technologie des Matériaux, Université Larbi Ben M'Hidi-Oum El Bouaghi, 04000 Oum El Bouaghi, Algeria*
[c]*Institut für Anorganische und Analytische Chemie, Technische Universität Braunschweig, Hagenring 30, 38106 Braunschweig, Germany*
[d]*Univ Rennes, CNRS, ISCR-UMR 6226, 35000 Rennes, France. E-mail: jean-yves.saillard@univ-rennes.fr*

† Electronic supplementary information (ESI) available. See DOI: https://doi.org/10.1039/d5nr01400j

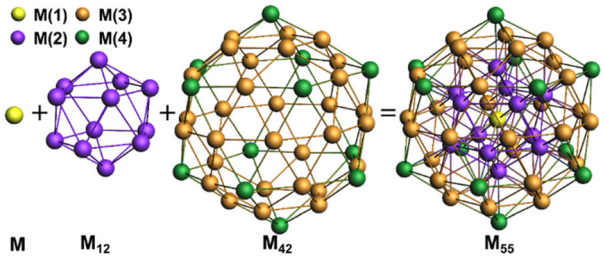

Fig. 1 The $M@M_{12}@M_{42} = Cu_{55}$ MacKay arrangement of I_h symmetry. Colors correspond to symmetry types. Note that the M_{42} outer shell is made of two interpenetrating polyhedra: An M_{30} icosidodecahedron (in yellow) and an M_{12} icosahedron (in green).

superatom.[15] Another one is Fischer's heterometallic open-shell 67-electron superatom $[(Cu_{43}Al_{12})Cp^*_{12}]$ ($Cp^* = \eta^5$-pentamethylcyclopentadienyl).[16] Very recently, Ohki and coworkers reported another paramagnetic M_{55} species, namely $[Fe_{55}H_{46}(P^tBu_3)_{12}]^q$ (q unknown).[17] The fourth example is the N-heterocyclic carbene-protected (NHC-protected) nanocluster $[Cu_{55}(IDipp)_6]$ (IDipp = 1,3-bis(2,6-diisopropylphenyl)imidazol-2-ylidene, see Scheme 1), made by one of us,[18] and shown in Fig. 2. This latter species is unique for several reasons. One reason is that it is by far richer in electrons than most of the ligated Cu_n clusters known so far.[19] Indeed, it possesses 55 electrons (if considered neutral, *i.e.*, only Cu(0) atoms), whereas the majority of the ligated homometallic copper superatoms are 2-electron species, with an average Cu oxidation state close to +I.[19] $[Cu_{55}(IDipp)_6]$ also echoes Schmid's iconic $[Au_{55}(PPh_3)_{12}Cl_6]$ nanocluster.[20,21] Although synthesized in 1981, this compound has not yet been structurally characterized by single-crystal X-ray diffraction and its precise structure is still debated. Based on various experimental data, a cuboctahedral structure has been initially proposed,[21] although the icosahedral arrangement has also been suggested, from powder X-ray diffraction[22] and later supported by density functional theory (DFT) calculations.[23] A more recent structural investigation, based on aberration-corrected scanning transmission electron microscopy, concluded that Schmid's cluster is in fact a mixture of several compounds, of which those approaching the $[Au_{55}(PPh_3)_{12}Cl_6]$ composition are a mixture of amorphous structures and an hybrid structure containing both cuboctahedral and icosahedral geometrical motifs.[24]

Finally, it should be noted that $[Cu_{55}(IDipp)_6]$ could be obtained only in a minuscule amount so that it was characterized only through single-crystal X-ray diffraction[18] and consequently its precise composition (and electric charge) is somewhat subject to doubt, in particular with respect to the possible presence of hydride ligands or of undetected disordered light counterions in the crystal structure. We report below a density functional theory (DFT) investigation at the BP86-D3/TZP level (see Computational details below) of $[Cu_{55}(IDipp)_6]$ and, in a more general way, of the Cu_{55} icosahedral arrangement, with a particular emphasis on the search for the electron count(s) that best favor(s) this so far rarely observed architecture. Related gold models are also explored for comparison and for its relationship with the hypothetical Schmid cluster. Finally, it is noteworthy that, if many computational investigations on hypothetical bare M_{55} (M = noble metal) icosahedral clusters have been performed in the past, almost all of them where considering neutral (and sometimes mono-ionic) species, without paying much attention on varying its electric charge in order to determine the electron count(s) that provide (s) the best closed-shell chemical stability to such architectures.

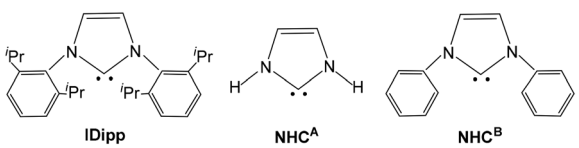

Scheme 1 The NHC ligands considered in this work.

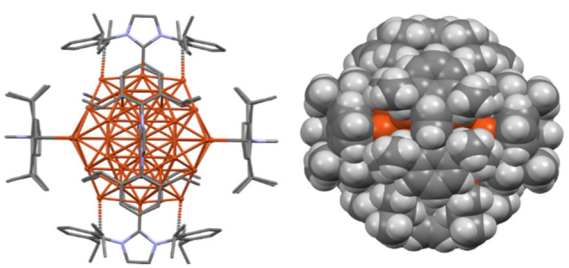

Fig. 2 The X-ray structure of $[Cu_{55}(IDipp)_6]$ (from ref. 23). Left: A stick view with hydrogen atoms omitted for clarity. The dashed lines represent the Cu···C long contacts. Right: A space-filling view.

2. Results and discussion

2.1. The bare Cu_{55} icosahedral architecture

We first investigate the electronic structure of the bare (unligated) $[Cu_{55}]$ cluster of I_h symmetry, for determining its most favored closed-shell electron count(s). Assuming the average Cu oxidation state to be as close as possible to zero, *i.e.*, a favored electron number as close as possible to 55 (only the 4s (Cu) electrons to be considered), the superatom model suggests a "magic" count of 58, corresponding to the closed-shell configuration $1S^2\ 1P^6\ 1D^{10}\ 2S^2\ 1F^{14}\ 2P^6\ 1G^{18}$,[4–6] that is, $[Cu_{55}]^{3-}$. However, the presence of a negative charge on the cluster is *a priori* questionable. Indeed, if one makes the approximation that metal–metal bonding is ensured only by the metal 4s(Cu) AOs, then such a compact delocalized structure is expected to generate a number of bonding MOs which is lower or equal to 56/2. Thus, more than 56 electrons should lead to the unfavorable occupation of antibonding orbitals. This crude reasoning does not account for the stabilizing effect caused by mixing with the 4p(Cu) AOs, which may damper the antibonding nature of the $[Cu_{55}]^{3-}$ HOMO, poss-

ibly to the point of rendering this electron count reachable. In any case, electron counts larger than 58 appear, at first sight, unlikely.

Symmetry considerations allow us to suggest *a priori* two additional possible electron counts. Indeed, the 9-fold degenerate 1G level in the R^3 symmetry group of the sphere, splits into two distinct levels in I_h symmetry, namely g_g (4-fold) and h_g (5-fold). A related symmetry splitting of the 1F level has been shown to exist in an Au_{32} icosahedral cluster.[25] Assuming significant splitting between the g_g and h_g levels, two potential closed-shell configurations can be suggested, $g_g^8\ h_g^0$ (48 electrons, $[Cu_{55}]^{7+}$) and $h_g^{10}\ g_g^0$ (50 electrons, $[Cu_{55}]^{5+}$). To complete the series, the electron counts of 52, 54 and 56 were also considered. They also correspond to partial occupation of the 1G level, but this time require Jahn–Teller distortions towards a lower than I_h symmetry. Moreover, for greater certainty regarding uttermost electron richness, the count of 60 electrons ($[Cu_{55}]^{5-}$) was also tested. Thus, seven closed-shell electron counts were considered. It tuned out that no low-energy closed-shell configuration could be found for the count of 54 electrons. On the other hand, significant HOMO–LUMO gaps (larger than 1.4 eV at the BP86-D3 level) were found for the six other electron counts. Their major results are gathered in Table 1 and their electronic configurations are sketched in Scheme 2. The corresponding Kohn–Sham orbital diagram of $[Cu_{55}]^{3-}$ (58 electrons), with the plots of its superatomic orbitals is shown in Fig. S1† and that of $[Cu_{55}]^-$ (56 electrons) is represented in Fig. 3. As expected, whereas the I_h symmetry is preserved for the 48, 50 and 58 counts, it is lowered to T_h for 52 and 56 electrons. In this symmetry group, the h_g and g_g irreducible representation of I_h split into $t_g + e_g$ and $t_g + a_g$, respectively. It turns out that both 52- and 56-electron counts can be derived from the I_h 58-electron case by a Jahn–Teller distortion issuing from partial depopulation of its g_g level, with the $a_g^2\ t_g^0$ and $t_g^6\ a_g^0$ configurations, respectively (Scheme 2). As for the 60-electron count, it corresponds simply to the addition of two electrons into the non-degenerate 3S (a_g) LUMO of the 58-electron species, thus maintaining the I_h symmetry of the cluster with the $1S^2\ 1P^6\ 1D^{10}\ 2S^2\ 1F^{14}\ 2P^6\ 1G^{18}\ 3S^2$

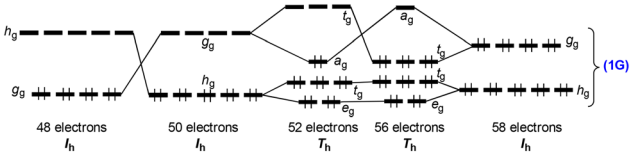

Scheme 2 Energy splitting, level ordering and orbital occupation for the icosahedral Cu_{55} architecture at various electron counts. Energy gaps are arbitrary.

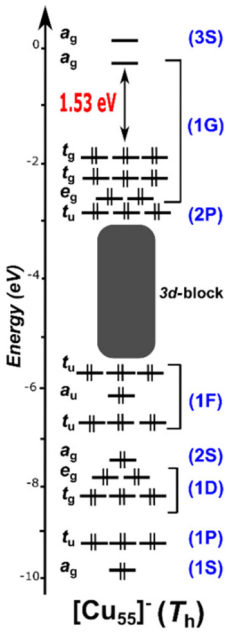

Fig. 3 Kohn–Sham orbital diagram of the 56-electron $[Cu_{55}]^-$ cluster.

superatomic configuration. It is however essential to mention that for this electron count, as well as for the count of 58, an important number of occupied orbitals are found to have positive energies, thus confirming the improbability of these two closed-shell electron counts, unlike the other four in which all

Table 1 Selected computed data for the closed-shell bare clusters $[Cu_{55}]^q$. q = +7, +5, +3, −1 and −3 correspond to the $1G^x$ (x = 8, 10, 12, 16 and 18 filling, respectively). q = −5 corresponds to the $1G^{18}\ 3S^2$ configuration. Cu–Cu distances (in Å) are averaged in the case of T_h symmetry. $\Delta E_{ico/cubo}$ is the energy difference between the icosahedral and cuboctahedral structures of the $[Cu_{55}]^q$ species

	$[Cu_{55}]^{7+}$	$[Cu_{55}]^{5+}$	$[Cu_{55}]^{3+}$	$[Cu_{55}]^-$	$[Cu_{55}]^{3-}$	$[Cu_{55}]^{5-}$
Superatomic electron count	48	50	52	56	58	60
Symmetry	I_h	I_h	T_h	T_h	I_h	I_h
1G splitting/occupation[a]	$g_g^8\ h_g^0$	$h_g^{10}\ g_g^0$	$e_g^4\ t_g^6\ a_g^2$	$e_g^4\ t_g^6\ t_g^6\ a_g^0$	$g_g^8\ h_g^{10}$	$g_g^8\ h_g^{10}\ a_g^2$
HOMO–LUMO gap (eV)	1.45	2.07	1.56	1.53	1.84	1.80
12 × Cu(1)–Cu(2)	2.474	2.438	2.421	2.410	2.411	2.411
30 × Cu(2)–Cu(2)	2.602	2.563	2.563	2.524	2.535	2.535
60 × Cu(2)–Cu(3)	2.485	2.494	2.464	2.531	2.524	2.524
40 × Cu(2)–Cu(4)	3.179	2.596	2.526	2.472	2.471	2.471
30 × Cu(3)–Cu(3)	2.610	2.604	2.588	2.614	2.617	2.617
60 × Cu(3)–Cu(4)	3.030	2.647	2.589	2.578	2.568	2.568
$\Delta E_{ico/cubo}$ (eV)	−10.18	−10.02	−8.27	−7.36	−7.18	−6.77

[a] $1G^{18}\ 1S^2$ in the case of $[Cu_{55}]^{5-}$.

occupied orbitals lie at substantially negative energies. It turns out that in all our ligated models described below, the same situation of positive energies for many occupied orbitals were found for the 58 and 60 electron counts, thus definitively ruling out these two numbers, which will not be discussed further in this paper.

2.2. The $Cu_{55}L_6$ and $Cu_{55}L_{12}$ models

We now turn to the ligated $[Cu_{55}(CO)_6]$ architecture, as a first-step simplified model for $[Cu_{55}(IDipp)_6]$ shown in Fig. 2.[18] In the latter, the IDipp ligands are linked to six among the 30 icosidodecahedron copper atoms (in yellow in Fig. 1). These particular six atoms are describing a regular octahedron, thus reducing the whole $[Cu_{55}(CO)_6]^q$ cluster ideal symmetry to T_h (see Fig. 4). In a similar way as for the $[Cu_{55}]^q$ series, all but one (q = +1; 54 electrons) electron counts provided significant HOMO–LUMO gaps, thus corresponding to 48, 50, 52 and 56 electrons (Table 2).

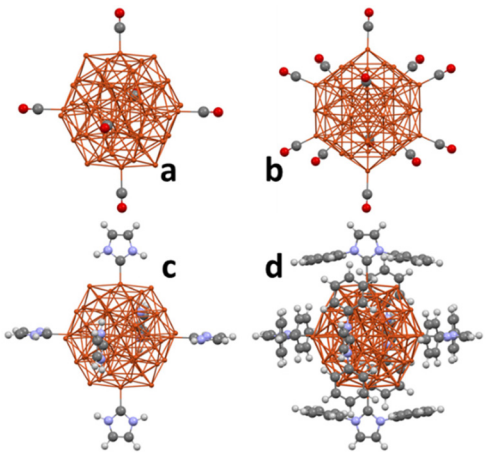

Fig. 4 The various computed models. (a) $[Cu_{55}(CO)_6]^q$; (b) $[Cu_{55}(CO)_{12}]^q$; (c) $[Cu_{55}(NHC^A)_6]^q$; (d) $[Cu_{55}(NHC^B)_6]^q$ (q = +7, +5, +3, −1).

They have similar closed-shell configuration as their bare homologues, except that the symmetry of the 48- and 50-electrons species is now reduced to T_h (see the Kohn–Sham orbital diagram of $[Cu_{55}(CO)_6]^-$ in Fig. S2†). Replacing the CO ligand by the simplest carbene model, *i.e.*, imidazolydene = NHC^A (see Scheme 1), to generate isoelectronic $[Cu_{55}(NHC^A)_6]^q$ clusters (Fig. 4) provided similar results as with carbonyl ligands (Table 2). Since the X-ray structure of $[Cu_{55}(IDipp)_6]$ exhibits non-bonding contacts (av. ~2.9 Å) between one carbon of each phenyl ring and its closest Cu neighbor (see left side of Fig. 1),[18] calculations were also performed with a simplified model of IDipp, where the ^{i}Pr groups were replaced by H *i.e.*, 1,3-diphenylimidazol-2-ylidene = NHC^B (see Scheme 1). Similar results as for NHC^A were obtained with NHC^B, and the Cu···C contacts were also reproduced for all the considered electron counts (Fig. 4 and Table 2). These weak interactions are indicative of the sterical protection provided by the ligands to the exposed copper atoms.

It is noteworthy that all the hexa-ligated series of models provided similar results, with the same four closed-shell configurations, among which those corresponding to 50 and 56 electrons present the largest HOMO–LUMO gaps. From the point of view of metrics, the 50-electron species $[Cu_{55}(NHC^B)_6]^{5+}$ has an overall slightly better agreement with the X-ray structure. Nevertheless, owing to the charge of the real $[Cu_{55}(IDipp)_6]$ cluster, we privilege the monoanionic state (56 electrons), which would assume the presence of an undetected cation (probably disordered) in the crystal structure. However, the possibility for a paramagnetic neutral species (55

Table 2 Selected computed data for the closed-shell $[Cu_{55}L_6]^q$ (L = CO, NHC^A, NHC^B) models. q = +7, +5, +3 and −1 correspond to the $1G^x$ (x = 8, 10, 12 and 16 filling, respectively). All distances (in Å) are averaged to I_h symmetry. $\Delta E_{ico/cubo}$ is the energy difference between the icosahedral and cuboctahedral structures of the $[Cu_{55}L_6]^q$ species. Experimental values of $Cu_{55}(IDipp)_6$ are also reported for comparison

	$[Cu_{55}L_6]^{7+}$			$[Cu_{55}L_6]^{5+}$			$[Cu_{55}L_6]^{3+}$			$[Cu_{55}L_6]^-$			$Cu_{55}(IDipp)_6$ (X-ray)[23]
L	CO	NHC^A	NHC^B	CO	NHC^A	NHC^B	CO	NHC^A	NHC^B	CO	NHC^A	NHC^B	
Superatomic electron count	48 50 52 56			50			52			56			55 (if neutral)
Symmetry	T_h T_h			T_h T_h			T_h T_h			T_h T_h			—
1G splitting/ occupation	$t_g^6 a_g^2$			$t_g^6 e_g^4$			$t_g^6 e_g^4$ a_g^2			$t_g^6 e_g^4$ t_g^6			—
HOMO–LUMO gap (eV)	1.30	1.30	1.44	1.86	1.76	1.94	1.25	1.30	1.44	2.05	1.68	1.86	—
Cu(1)–Cu(2)	2.443	2.455	2.450	2.437	2.449	2.536	2.415	2.444	2.437	2.405	2.443	2.432	2.450
Cu(2)–Cu(2)	2.546	2.555	2.557	2.543	2.543	2.613	2.522	2.542	2.539	2.523	2.551	2.538	2.550
Cu(2)–Cu(3)	2.691	2.504	2.543	2.501	2.575	2.594	2.491	2.565	2.547	2.469	2.560	2.504	2.495
Cu(2)–Cu(4)	2.895	2.454	2.467	2.570	2.449	2.495	2.530	2.440	2.424	2.515	2.438	2.406	2.399
Cu(3)–Cu(3)	2.692	2.669	2.641	2.602	2.650	2.667	2.589	2.646	2.636	2.597	2.652	2.635	2.603
Cu(3)–Cu(4)	2.781	2.593	2.589	2.633	2.589	2.650	2.602	2.582	2.536	2.580	2.583	2.549	2.548
Cu–C	1.943	2.000	1.997	1.963	2.003	1.996	1.920	2.003	2.021	1.884	1.985	1.978	1.969
Cu···C	—	—	2.751	—	—	3.036	—	—	—	2.878	—	—	2.924	2.883
$\Delta E_{ico/cubo}$ (eV)	−3.81	−3.49	−3.67	−4.18	−4.09	−4.28	−4.11	−3.67	−3.79	−2.09	−3.08	−3.27	—

electrons, see Table S1†) is not to be ruled out. Indeed, although its spin density is found to be mainly located on the Cu_{42} metal outer shell, it is efficiently screened by the IDipp covering sphere of ligands, as illustrated by the cluster space-filling view shown on the right side of Fig. 2. The efficiency of such a ligand screening has been also proven with Cp* ligands in the case of the paramagnetic $[(Cu_{43}Al_{12})Cp^*_{12}]$.[21]

Owing to the fact that in the above-considered $Cu_{55}L_6$ models, the ligands have little effect on the superatomic electronic structure of the cluster, we also tested a situation with a different number of neutral carbonyl ligands (twelve) and a different configuration of the latter (bonded to the twelve green Cu atoms in Fig. 1), which does not break the ideal I_h symmetry (see Fig. 4). It turn out that the results on these $[Cu_{55}(CO)_{12}]$ models (Table 3) were found to be quite similar to those obtained for the $Cu_{55}L_6$ series (Table 2). One can thus conclude that several favored electron counts are possible for the icosahedral Cu_{55} arrangement, which are moderately dependent from the electronic effect of the ligands. However, the formal charges of the ligands are important in the sense that formally anionic ligands (*e.g.* halides, thiolates, alkynyls, *etc.*) are expected to stabilize the lowest electron counts (48, 50 and 52).

2.3. Au_{55} *vs.* Cu_{55} species

The recent interest for NHC-stabilized gold nanoclusters,[26] as well as the controversy over the nature of Schmid's $[Au_{55}(PPh_3)_{12}Cl_6]$ cluster (see above), prompted us to undertake a comparison between gold and copper in these icosahedral arrangements. First of all, it is to be noted that, in the case of all the considered bare and ligated Cu_{55} species discussed above, the icosahedral arrangement was found to be much more stable than its cuboctahedral counterpart for all the considered electron counts (Tables 1–3). A similar result was found for the closed-shell electron counts of the $[Au_{55}]^q$ series (Table 4). However, the differences in energy between both structural arrangements, although still significant, were found smaller in the gold case. It is also to be noted that no low-energy closed-shell configuration could be found for the count of 54 electrons, as in the case of its copper analogue (see above), but also for the count of 52 electrons. As for copper, a substantial number of occupied orbitals with positive energies was found in the case of 58 and 60 electrons, thus ruling out these two electron numbers, which are not to be discussed further. Adding six NHC ligands in

Table 3 Selected computed data for the closed-shell $[Cu_{55}(CO)_{12}]^q$ models. q = +7, +5, +3 and −1 correspond to the $1G^x$ (x = 8, 10, 12 and 16 filling, respectively). All Cu–Cu distances (in Å) are averaged to I_h symmetry. $\Delta E_{ico/cubo}$ is the energy difference between the icosahedral and cuboctahedral structures

	$[Cu_{55}(CO)_{12}]^{7+}$	$[Cu_{55}(CO)_{12}]^{5+}$	$[Cu_{55}(CO)_{12}]^{3+}$	$[Cu_{55}(CO)_{12}]^{-}$
Superatomic electron count	48	50	52	56
Symmetry	I_h	I_h	T_h	T_h
1G splitting/occupation	$g_g^8\ h_g^0$	$h_g^{10}\ g_g^0$	$t_g^6\ e_g^4\ a_g^2$	$t_g^6\ e_g^4\ t_g^6$
HOMO–LUMO gap (eV)	1.40	1.79	1.48	1.46
Cu(1)–Cu(2)	2.452	2.468	2.460	2.540
Cu(2)–Cu(2)	2.578	2.595	2.587	2.658
Cu(2)–Cu(3)	2.530	2.516	2.514	2.552
Cu(2)–Cu(4)	2.487	2.539	2.512	2.534
Cu(3)–Cu(3)	2.637	2.630	2.620	2.676
Cu(3)–Cu(4)	2.597	2.633	2.614	2.662
Cu–C	1.904	2.103	1.975	1.925
$\Delta E_{ico/cubo}$ (eV)	−10.12	−9.81	−9.50	−8.91

Table 4 Selected computed data for the closed-shell $[Au_{55}]^q$ and $[Au_{55}L_6]^q$ (L = NHC^A, NHC^B) models. q = +7, +5 and −1 correspond to the $1G^x$ (x = 8, 10 and 16 filling, respectively). All distances (in Å) are averaged to I_h symmetry

	$[Au_{55}]^{7+}$	$[Au_{55}L_6]^{7+}$		$[Au_{55}]^{5+}$	$[Au_{55}L_6]^{5+}$		$[Au_{55}]^{-}$	$[Au_{55}L_6]^{-}$	
L	—	NHC^A	NHC^B	—	NHC^A	NHC^B	—	NHC^A	NHC^B
Superatomic electron count	48			50			56		
Symmetry	I_h	T_h		I_h	T_h		I_h	T_h	
1G splitting/occupation	$g_g^8\ h_g^0$	$t_g^6\ a_g^2$		$h_g^{10}\ g_g^0$	$t_g^6\ e_g^4$		$t_g^6\ e_g^4\ t_g^6$		
HOMO–LUMO gap (eV)	1.46	1.35	1.48	2.05	1.81	1.86	1.46	2.10	1.99
Au(1)–Au(2)	2.769	2.780	2.785	2.761	2.766	2.757	2.746	2.775	2.770
Au(2)–Au(2)	2.911	2.977	2.975	2.903	2.940	2.932	2.887	2.939	2.919
Au(2)–Au(3)	2.866	2.912	2.955	2.863	2.899	2.867	2.879	2.927	2.900
Au(2)–Au(4)	2.805	2.758	2.753	2.775	2.776	2.766	2.740	2.765	2.755
Au(3)–Au(3)	2.982	3.028	3.074	2.977	3.008	2.998	2.983	3.007	2.999
Au(3)–Au(4)	2.932	2.920	2.928	2.913	2.916	2.902	2.913	2.915	2.901
Au–C	—	2.078	2.054	—	2.054	2.003	—	2.067	2.001
Au···C	—	—	2.599	—	—	2.678	—	—	2.789
$\Delta E_{ico/cubo}$ (eV)	−1.77	−4.14	−3.96	−2.27	−4.01	−3.85	−1.79	−1.96	−1.90

the same way as in the case of the copper species provided similar results as for the bare Au_{55} species (Table 4). Assuming the exact $[Au_{55}(PPh_3)_{12}Cl_6]$ composition for Schmid cluster, it is a 49-electron species, a count intermediate between two favored closed-shell situations, of which the count of 50 appears privileged from the HOMO/LUMO gap point of view, as previously noted by Muñoz-Castro,[27] although this compound most likely has a more complex structure and/or composition.[23,24]

3. Concluding remarks

Our calculations predict four favorable closed-shell electron counts (48, 50, 52 and 56) susceptible to stabilize a ligand-protected nanocluster with icosahedral Cu_{55} core. Electron-counts lower than 48 were not explored and may remain possible (*e.g.* 40), but those larger than 56 were found not to be allowed. This last result is in line with a former computational investigation on Schmid-type related gold clusters, which found that the 58-electron count is unlikely for the Au_{55} species and predicted it to be best favored for a cluster of larger nuclearity, namely $[Au_{69}(PR_3)_{20}Cl_{12}]^-$.[28] As for the experimentally reported $[Cu_{55}(IDipp)_6]$ compound,[18] its composition is fully confirmed by our calculations, which show that it is either a 56-electron mono-anion, or a paramagnetic 55-electron neutral species. In any case, the presence of no more than six bulky NHC ligands is enough to provide the metallic core with a full coverage of its surface, the "exposed" copper atoms being in fact hidden below the outer compact ligand sphere. Thus, chemical stability does not necessitate that each surface metal atom should be saturated by covalently bonding to one (or more) ligand(s), but the ligand shell should be compact enough to sterically protect the "exposed" metals, if any. From this perspective, our crude carbonyl models are unlikely to exist, but large phosphine and/or thiolate ligands, for example, constitute good candidates to stabilize one of the four predicted electron counts. Note that a test calculation on the simple thiolate-protected 50-electron model $[Cu_{55}(HS)_6]^-$ provided similar results as for its isoelectronic $[Cu_{55}(CO)_6]^{5+}$ relative (Table S1†).

Similar results are obtained with gold homologues, except that this time the closed-shell count of 52 electrons is not allowed. Thus, $[Au_{55}(IDipp)_6]^-$ should be viable.[29] The hypothetical $[Au_{55}(PR_3)_{12}Cl_6]$ composition of Schmid's cluster matches well with the favored closed-shell counts of 48 and 50[27] electrons, assuming a mono-ionic state, knowing that other non-icosahedral architectures are competing for this hypothetical compound.[23,24,28] In any case, our results here support the fact that there is a large variety of ligand shells, both in terms of composition and configuration, that are able to stabilize the icosahedral M_{55} (M = group 11 metal) core. It is however to note that electron counts much lower than those explored in this work can favor a different structural arrangement, as exemplified by the 28-electron $[Au_{55}(SC_6H_4Me)_{24}(Ph_3P)_6]^{3+}$, which features a face-centered cubic (fcc) Au_{55} core.[30]

4. Computational details

DFT calculations were performed with the use of the Amsterdam Density Functional code (ADF2020.01),[31] incorporating scalar relativistic corrections *via* the zeroth-order regular approximation (ZORA) Hamiltonian.[31,32] The BP86 functional[33–37] was used, with the addition of Grimme's D3 empirical corrections,[37,38] to take into account dispersion effects. A Slater-type orbital basis sets of triple-zeta plus one polarization function (STO-TZP) quality was considered.[39] The frozen-core approximation was used to treat the core shells up to 1s for C and N, 2p for P and Cl, 3p for Cu and 5p for Au. Full geometry optimizations were performed using the analytical gradient method implemented by Versluis and Ziegler.[40] Vibrational frequency calculations[41,42] were performed on all the optimized models to check that their geometries correspond to minima on the potential energy surface.

Data availability

The data supporting the findings of this study are available within the article and its ESI.† Complementary raw data are available from the corresponding author, upon reasonable request.

Conflicts of interest

There are no conflicts to declare.

Acknowledgements

MAZ and BZ acknowledge the Universities Mentouri (Constantine 1) and Larbi Ben M'Hidi (Oum El Bouaghi). JYS acknowledges the University of Rennes and the CNRS.

References

1 X. Kang, Y. Li, M. Zhu and R. Jin, *Chem. Soc. Rev.*, 2020, **49**, 6443–6514.
2 S. Qian, Z. Wang, Z. Zuo, X. Wang, Q. Wang and X. Yuan, *Coord. Chem. Rev.*, 2022, **451**, 214268.
3 J. Wang, P. Li, C. Wang, N. Liu and D. Xing, *Mater. Horiz.*, 2023, **10**, 3304–3324.
4 S. N. Khanna and P. Jena, *Phys. Rev. B: Condens. Matter Mater. Phys.*, 1995, **51**, 13705–13716.
5 M. Walter, J. Akola, O. Lopez-Acevedo, P. D. Jadzinsky, G. Calero, C. J. Ackerson, R. L. Whetten, H. Grönbeck and H. Häkkinen, *Proc. Natl. Acad. Sci. U. S. A.*, 2008, **10**, 9157–9162.
6 F. Gam, J. Wei, S. Kahlal, J.-Y. Saillard and J.-F. Halet, *Struct. Bonding*, 2021, **188**, 69–102.
7 A. L. Mackay, *Acta Crystallogr.*, 1962, **15**, 916–918.

8 C. E. Briant, B. R. C. Theobald, J. W. White, L. K. Bell, D. M. P. Mingos and A. J. Welch, *J. Chem. Soc., Chem. Commun.*, 1981, 201–202.
9 N. T. Tran, D. R. Powell and L. F. Dahl, *Angew. Chem., Int. Ed.*, 2000, **39**, 4121–4125.
10 E. G. Mednikov, M. C. Jewell and L. F. Dahl, *J. Am. Chem. Soc.*, 2007, **129**, 11619–11630.
11 A. Dass, S. Theivendran, P. R. Nimmala, C. Kumara, V. R. Jupally, A. Fortunelli, L. Sementa, G. Barcaro, X. Zuo and B. C. Noll, *J. Am. Chem. Soc.*, 2015, **137**, 4610–4613.
12 M. Strienz, A. Poddelskii, B. K. Moll, C. Schrenk, P. S. Thomas, A. Z. Clayborne and A. Schnepf, *Angew. Chem., Int. Ed.*, 2025, **64**, e202500586.
13 F. Hu, Z.-J. Guan, S.-F. Yuan and Q.-M. Wang, *Chem. – Asian J.*, 2023, **18**, e202300605.
14 J. D. Erickson, E. G. Mednikov, S. A. Ivanov and L. F. Dahl, *J. Am. Chem. Soc.*, 2016, **138**, 1502–1505.
15 J. Wei, R. Marchal, D. Astruc, J.-Y. Saillard, J.-F. Halet and S. Kahlal, *Chem. – Eur. J.*, 2020, **26**, 5508–5514.
16 J. Weßing, C. Ganesamoorthy, S. Kahlal, R. Marchal, C. Gemel, O. Cador, A. C. H. Da Silva, J. L. F. Da Silva, J.-Y. Saillard and R. A. Fischer, *Angew. Chem., Int. Ed.*, 2018, **57**, 14630–14634.
17 T. Higaki, K. Tanaka, H. Izu, S. Oishi, K. Kawamoto, M. Tada, W. M. C. Sameera, R. Takahata, T. Teranishi, S. Kikkawa, S. Yamazoe, T. Shiga, M. Nihei, T. Kato, R. E. Cramer, Z. Zhang, K. Meyer and Y. Ohki, *J. Am. Chem. Soc.*, 2025, **147**, 3215–3222.
18 W. Drescher, C. Borner and C. Kleeberg, *New J. Chem.*, 2021, **45**, 14957–14964.
19 B. Zouchoune and J.-Y. Saillard, *Molecules*, 2024, **29**, 605.
20 G. Schmid, R. Boese, R. Pfeil, F. Bandermann, S. Mayer, G. H. M. Calis and J. W. A. van der Velden, *Chem. Ber.*, 1981, **114**, 3634–3642.
21 G. Schmid, *Chem. Soc. Rev.*, 2008, **37**, 1909–1930.
22 W. Vogel, B. Rosner and B. Tesche, *J. Phys. Chem.*, 1993, **97**, 11611–11616.
23 Y. Pei, N. Shao, Y. Gao and X. Zeng, *ACS Nano*, 2010, **4**, 2009–2020.
24 N. Jian, C. Stapelfeldt, K.-J. Hu, M. Fröba and R. E. Palmer, *Nanoscale*, 2015, **7**, 885–888.
25 S. Kenzler, F. Fetzer, C. Schrenk, N. Pollard, A. R. Frojd, A. Z. Clayborne and A. Schnepf, *Angew. Chem., Int. Ed.*, 2019, **23**, 5902–5905.
26 E. L. Albright, T. I. Levchenko, V. K. Kulkarni, A. I. Sullivan, J. F. DeJesus, S. Malola, S. Takano, M. Nambo, K. Stamplecoskie, H. Häkkinen, T. Tsukuda and C. M. Crudden, *J. Am. Chem. Soc.*, 2024, **146**, 5759–5780.
27 A. Muñoz-Castro, *ChemPhysChem*, 2025, **26**, e202400892.
28 M. Walter, M. Moseler, R. L. Whetten and H. Häkkinen, *Chem. Sci.*, 2011, **2**, 1583–1587.
29 R. Hoffmann, P. von Ragué Schleyer and H. F. Schaefer III, *Angew. Chem., Int. Ed.*, 2008, **47**, 7164–7167.
30 X.-K. Wan, J.-Q. Wang and Q.-M. Wang, *Angew. Chem., Int. Ed.*, 2021, **60**, 20748–20753.
31 G. te Velde, F. M. Bickelhaupt, E. J. Baerends, C. Fonseca Guerra, S. J. A. van Gisbergen, J. G. Snijders and T. Ziegler, *J. Comput. Chem.*, 2001, **22**, 931–967.
32 E. van Lenthe, E. J. Baerends and J. G. Snijders, *J. Chem. Phys.*, 1993, **99**, 4597–4610.
33 A. D. Becke, *J. Chem. Phys.*, 1986, **84**, 4524–4529.
34 A. D. Becke, *Phys. Rev. A*, 1988, **38**, 3098–3100.
35 J. P. Perdew, *Phys. Rev. B: Condens. Matter Mater. Phys.*, 1986, **33**, 8822–8824.
36 J. P. Perdew, *Phys. Rev. B: Condens. Matter Mater. Phys.*, 1986, **34**, 7406–7406.
37 S. Grimme, *J. Comput. Chem.*, 2006, **27**, 1787–1799.
38 S. Grimme, J. Antony, S. Ehrlich and H. Krieg, *J. Chem. Phys.*, 2010, **132**, 154104.
39 J. E. van Lenthe and E. J. Baerends, *J. Comput. Chem.*, 2003, **24**, 1142–1156.
40 L. Versluis and T. Ziegler, *J. Chem. Phys.*, 1988, **88**, 322–329.
41 L. Fan and T. Ziegler, *J. Chem. Phys.*, 1992, **96**, 6937–6941.
42 L. Fan and T. Ziegler, *J. Chem. Phys.*, 1992, **96**, 9005–9012.